Available online at www.sciencedirect.com

ScienceDirect

Procedia CIRP 122 (2024) 683–688

www.elsevier.com/locate/procedia

31st CIRP Conference on Life Cycle Engineering (LCE 2024)

# A multi-objective optimization workflow of ring-rolling process parameters based on production energy and time

Cristian Cappellini[a]*, Claudio Giardini[a], Sara Bocchi[a]

[a]*University of Bergamo, Department of Management, Information and Production Engineering, Via Pasubio 7/b, 24044 Dalmine, Italy*

* Corresponding author. Tel.: +39-035-2052305; fax: +0-000-000-0000. *E-mail address:* cristian.cappellini@unibg.it

**Abstract**

Our industrial era is characterized by a significant attention to environmental aspects and production sustainability. Under this point of view, the minimization of the process energy represents a milestone leading to a consistent reduction of pollution. However, to promptly react to the high production rate market request, companies employ time saving manufacturing strategies, often in contrast with this principle. Considering this, an optimization concerning the reduction of both production time and energy, results to be strategical, especially when energy-intensive processes, such as ring rolling, are considered. Ring rolling is a shaping process performed by a dedicated equipment, composed of a driving roll, an idle roll, and a couple of axial rolls, allowing to obtain seamless rings while simultaneously reducing their height and thickness, while enlarging diameter. The kinematics of each component of the equipment can be set independently. This leads to several process conditions influencing quality, energy, and times, and makes it difficult the selection of the most suitable configuration. In this paper, a multi-objective optimization workflow is presented. Starting from validated FEM simulation campaign results, the proposed methodology allowed to individuate the best process parameters combination for limiting energy and time, encouraging its application to a wider range of energy-consuming processes.

© 2024 The Authors. Published by Elsevier B.V.
This is an open access article under the CC BY-NC-ND license (https://creativecommons.org/licenses/by-nc-nd/4.0)
Peer-review under responsibility of the scientific committee of the 31st CIRP Conference on Life Cycle Engineering (LCE 2024)

*Keywords:* Ring rolling; Multi-objective optimization; Process sustainability

## 1. Introduction

In the last decades, increasing attention has been dedicated to increasing production sustainability by limiting energy consumption and containing pollution [1]. The importance of this aspect increases when energy-consuming processes are involved, where even a small percentage of energy reduction, represents a great advantage for the environment [2]. However, this principle is rarely fully applied by industries, due to production rate maximization required by the market [3]. Hence, the possibility of employing simple tools capable of simultaneously optimizing different factors, in addition to process time, represents a tactical task [4].

Hot deformation manufacturing covers a wide range of energy-intensive processes, such as forging, cogging, shape and ring rolling (RR). This latter concerns the processing of a ring-shaped workpiece using a dedicated equipment consisting of a motorized rotating driving roll, an idle mandrel that moves radially towards the driving roll, and a couple of conical rolls that compress the ring axially. The combined action of these rolls induces a state of radial-axial deformation permitting a diametral growth through a reduction of its thickness and height, up to the desired ring dimensions [5]. Thanks to RR capability of processing a great variety of materials [6,7], it is widely employed in energetics, oil and gas, aero-space, and transportation fields, to produce large seamless rings [8]. Furthermore, in comparison with other processes, RR results advantageous in terms of surface quality, material savings, microstructure orientation, and no need of post-heat treatments [9].

Despite this, due to the complexity of the state of deformation, the influence of rolling parameters must be deeply

2212-8271 © 2024 The Authors. Published by Elsevier B.V.
This is an open access article under the CC BY-NC-ND license (https://creativecommons.org/licenses/by-nc-nd/4.0)
Peer-review under responsibility of the scientific committee of the 31st CIRP Conference on Life Cycle Engineering (LCE 2024)
10.1016/j.procir.2024.01.095

analyzed, to obtain high quality products. Under this point of view, scholars exploiting slip-line field theory [10], artificial neural networks [11], regression models [12], and finite element method (FEM) [13] were proposed. However, most of these studies only focuses on separate ring quality attributes, while poor is the bibliography concerning multiple aspects related to quality, energy, and process time. In [14] rolling temperature and mandrel feed were simultaneously optimized by the maximization of a dedicated formability index. In another work [15], fishtail effects were reduced by improving the design of equipment components based on the deformation zone geometry and strain distribution. An objective function defined as the combination of strain, temperature, and deformation trajectory, was proposed in [16] to optimize grain size and loads.

Focusing attention on the process sustainability, the present paper proposes a multi-objective optimization of RR based on energy consumption, driving roll torque, ring quality, and production time. For developing it, a simulative campaign based on an already validated FEM model, was planned by varying five levels of two rolling parameters, namely mandrel feed and ring rotational speed. The achieved values of energy, maximum driving roll torque, ring quality, and production time, have been arranged to define the objective function that, once minimized, has allowed to identify the optimized combination of process parameters. The results obtained are encouraging, suggesting the possibility of applying the proposed methodology to wider range of more sustainable energy-consuming processes.

## 2. Multi-objective optimization workflow

In the present paper, the proposed multi-objective optimization workflow was applied to a ring rolling process, since it is considered to be an energy-intensive one.

In the first step of the workflow, the RR parameters (inputs), and the responses (outputs), most influencing the process sustainability, are selected. The related experimental plan is then designed by varying the inputs on different levels. After the collection of the experimental responses, these are arranged in an objective function. The minimization of the objective function will result in the optimum process parameters combination. The following paragraphs describe how the workflow was developed in the analyzed case study.

## 3. Materials and methods

### *3.1. Simulation plan and setup*

The simulation plan was designed considering two factors (namely, mandrel feed rate $F$ [mm/s] and ring rotational speed $\omega_r$ [rad/s]) that have been varied on 5 different levels as reported in Table 1. The FEM model used for carrying out the process simulations has been already validated in a previous research paper [17].

The simulations were performed using the ring rolling guided using interface (GUI) of the simulation software. This GUI concerns a dedicated arbitrary Lagrangian-Eulerian (ALE) solver reducing the computational times.

Table 1. The simulation plan considered.

| Process parameter | Levels | | | | |
|---|---|---|---|---|---|
| $F$ [mm/s] | 0.50 | 0.75 | 1.00 | 1.25 | 1.50 |
| $\omega_r$ [rad/s] | 5 | 10 | 15 | 20 | 25 |

Figure 1 shows the simulation setup where $F$, $\omega_r$, the rotational speed of the driving roll $\omega_{DR}$, and the conical roll axial speed $f_{AR}$ are represented. In Figure 2a the geometric features of the ring, its cross-section variation from the beginning to the end of the process and the related rolling curve are reported. The rolling curve represents the simultaneous values of ring height ($H$) and width ($W$) during RR. The same rolling curve was employed for all the simulations, and it is shown in detail in Figure 2b.

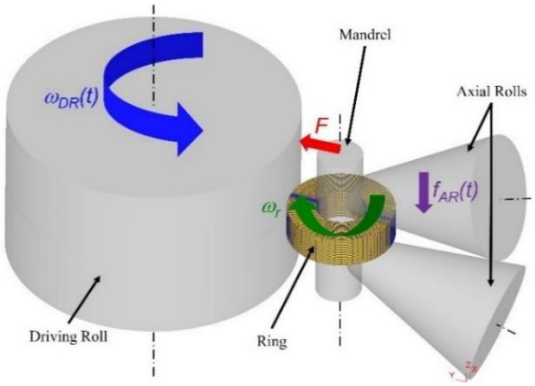


Fig. 1. Simulation setup and rolling curve.

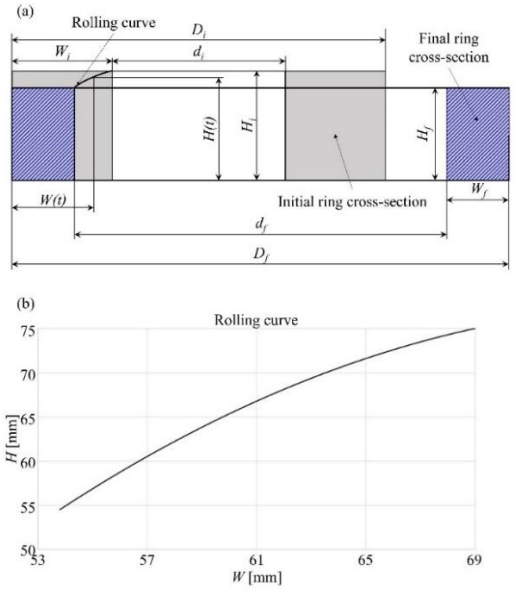


Fig. 2. (a) Ring dimensions and cross-sectional variation during RR, (b) the rolling curve employed in the simulations.

Table 2 reports initial and final theorical dimensions of the ring. The driving roll, the mandrel, and the conical axial roll were considered perfectly rigid bodies. The diameters of the driving roll $D_{DR}$ and of the mandrel were 700 mm and 110 mm respectively, while the axial roll taper angle was 15.7°.

Table 2. Initial and final theorical dimensions of the ring.

| | Initial dimension | Final dimension |
|---|---|---|
| Outer diameter [mm] | $D_i = 258$ | $D_f = 387.39$ |
| Inner diameter [mm] | $d_i = 120$ | $d_f = 279.79$ |
| Width [mm] | $W_i = 69$ | $W_f = 53.8$ |
| Height [mm] | $H_i = 75$ | $H_f = 54.5$ |

The ring was discretized with a mesh of 14,500 hexahedral elements refined in the contact area with the equipment components. The ring was modeled as a viscous-plastic AISI 1045 steel material; the stress-strain law was taken from the internal simulation database. The friction on the contact interfaces was considered using a shear model with a friction factor equal to 0.7. The kinematics of the equipment were derived considering the rolling curve and the ring volume constancy. Hence, the ring width evolution $W(t)$ is represented by Eq. (1)

$$W(t) = W_i - F \cdot t \tag{1}$$

From the $F$ value it is possible to calculate the process duration $t_{RR}$ [s] according to Eq. (2):

$$t_{RR} = \left(W_i - W_f\right)/F = \Delta W/F \tag{2}$$

The axial roll speed $f_{AR}(t)$ [mm/s] was selected as linearly increasing during the process. The initial value of $f_{ARi}$ was set to half of the mean value of the speed to cover the height reduction $\Delta H$ (Eq. (3)).

$$f_{ARi} = \frac{1}{2}\frac{\left(H_i - H_f\right)}{t_{RR}} = \Delta H/2t_{RR} \tag{3}$$

The axial speed ratio $m$ was determined by equaling the integral of $f_{AR}(t)$ along $t_{RR}$ to the height reduction $\Delta H$ (Eq. (4)):

$$\int_0^{t_{RR}} f_{AR}\,dt = \int_0^{t_{RR}} (f_{ARi} + m \cdot t)dt = \Delta H \rightarrow m = \frac{\Delta H}{2t_{RR}^2} \tag{4}$$

Therefore, $f_{AR}(t)$ can be derived as reported in Eq. (5), leading to the instantaneous ring height $H(t)$ of Eq. (6):

$$f_{AR}(t) = f_{ARi} + m \cdot t = (\Delta H/2t_{RR}) + (\Delta H/2t_{RR}^2)t \tag{5}$$

$$H(t) = H_i - (\Delta H/2t_{RR})t + (\Delta H/2t_{RR}^2)t^2 \tag{6}$$

Once $W(t)$ and $H(t)$ are known, the growth of the outer diameter $D(t)$ can be calculated as reported in Eq. (7) considering the volume constancy:

$$D(t) = W(t) + \frac{H_i(D_i^2 - d_i^2)}{4H(t)W(t)} \tag{7}$$

In absence of sliding condition, the instantaneous driving roll rotational speed $\omega_{DR}(t)$ is determined by equaling ring and driving roll tangential speeds (Eq. (8)):

$$\omega_{DR}(t) = \frac{\omega_r}{D_{DR}}D(t) = \frac{\omega_r}{D_{DR}}D(t)\left[W(t) + \frac{H_i(D_i^2 - d_i^2)}{4H(t)W(t)}\right] \tag{8}$$

For each combination of process parameters in Table 1, $f_{AR}(t)$ and $\omega_{DR}(t)$ calculated according to Eqs. (5) and (8) were implemented in the simulation software as motion laws of axial and driving rolls. The constant radial speed $F$ was assigned to the mandrel. Since the rotations of mandrel and axial rolls around their axes are free, the related resistant torque was set to the null value. The ring temperature was 1150°C and, due to the low process time, the simulations were carried out in isothermal conditions.

### 3.2. Collection, selection, and calculation of process outputs

Four responses, differently affecting the process sustainability, were selected:

- the total energy necessary to complete the process, $E$ [Nm];
- the maximum driving roll torque, $T_{max}$ [Nm], influencing the motor dimensions and costs;
- the process duration, $t_{RR}$ [s];
- the geometric ring quality $Q$, leading, if not respected, to the need of post-processing operations.

The $E$ was calculated by applying Eq. (9):

$$E = \int_0^{t_{RR}} [F_r(t) \cdot F + F_a(t) \cdot f_{AR}(t) + T(t) \cdot \omega_{DR}(t)]dt \tag{9}$$

where $F_r(t)$ [N], $F_a(t)$ [N], and $T(t)$ [Nm] are the evolution during the simulation of mandrel radial force, conical roll axial force $F_a(t)$ [N], and driving roll torque $T(t)$ [Nm], respectively.

The $T_{max}$ value was also recorded.

To individuate the most restrictive geometric feature, in terms of quality, a preliminary analysis of $W_f$, $H_f$, and $D_f$, was performed. For each feature of every simulation, a precision parameter was calculated as reported in Eq. (10):

$$\%p_{feat} = \frac{|feat - feat_{sim}|}{feat} \cdot 100\% \tag{10}$$

where $feat$ alternatively indicates one of the geometric features ($W_f$, $H_f$, or $D_f$), while $feat_{sim}$ the value of the same feature ($W_{f\_sim}$, $H_{f\_sim}$, or $D_{f\_sim}$) measured in the simulation. Considering Eq. (10), a lower value of $\%p_{feat}$ corresponds to a simulated value closer to the theorical one, indicating a better quality of the feature. The contour plots of $\%p_{Df}$, $\%p_{Hf}$, and $\%p_{Wf}$, for the combinations of the rolling parameters are visible in Figure 3. In these plots, each precision level highlights a determined area. It is possible to observe that for each precision level of $\%p_{Df}$, the highlighted areas corresponding to the same levels of $\%p_{Hf}$ and $\%p_{Wf}$ are smaller. As an example, the subtended areas for a precision value of 1% are contoured. This means that, once a determined quality of $D_{f\_sim}$ will be reached, the tolerances obtained for $H_{f\_sim}$ and $W_{f\_sim}$ will be narrower, revealing $D_{f\_sim}$ as the most restrictive geometric feature.

In consideration of this, the geometric ring quality parameter $Q$ was defined as the ratio between $D_{f\_sim}$ and the desired $D_f$, as reported in Eq. (11), indicating a good quality when $Q$ is closed to the unity.

$$Q = D_{f\_sim}/D_f \quad (11)$$

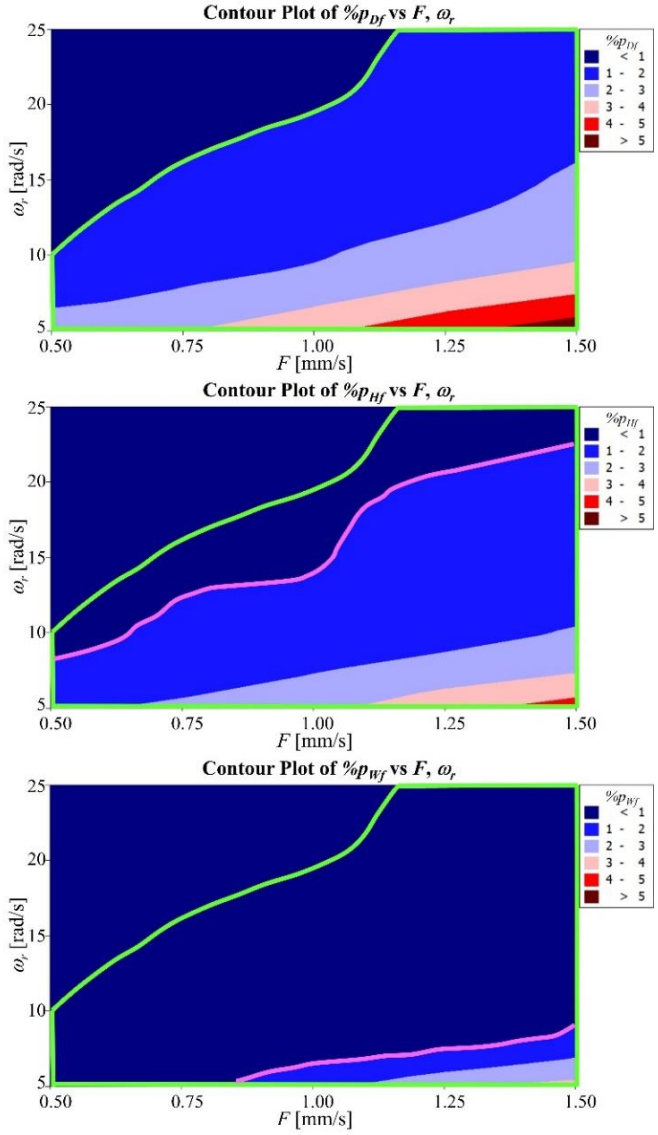


Fig. 3. Contour plots of the precision parameters defined by Eq. (10) for: (a) $D_{f\_sim}$, (b) $H_{f\_sim}$, and (c) $W_{f\_sim}$. The subtended areas for a precision level of 1% are highlighted.

Referring to Eq. (2), it is evident how $t_{RR}$ assumes the maximum value for the lowest value of $F$, and vice versa.

Figure 4 reports the behavior of $E$ (Figure 4a), $T_{max}$ (Figure 4b), and $Q$ (Figure 4c) as $F$ and $\omega_r$ vary.

The opposite trends of $E$ and $T_{max}$ are visible in Figures 4a-b. An intensification of $F$, in fact, leads to an energy diminution and a $T_{max}$ growth. Contrarily, the higher the $\omega_r$, the greater the energy consumption and the lower the $T_{max}$. For better understand this behavior, Figure 5 reporting the torque $T(t)$ evolution during process time for the combinations of the extreme process parameters values of the plan, has been added. As reported by Eq. (8), a higher $\omega_r$ implicates a higher $\omega_{DR}$. Despite an intensification of $\omega_r$ reduces $T_{max}$, this decrease does not compensate the $\omega_{DR}$ growth, making the energy consumption increasing. Again, an increase of $F$ results in a $T_{max}$ growth due to a higher contact area between the driving roll and the ring. In addition, a reduction of $t_{RR}$ is obtained. The diminution of the process time has a greater effect on $E$ respect to the intensification of the torque. As a result, when increasing $F$, a reduction of $E$ is noticeable.

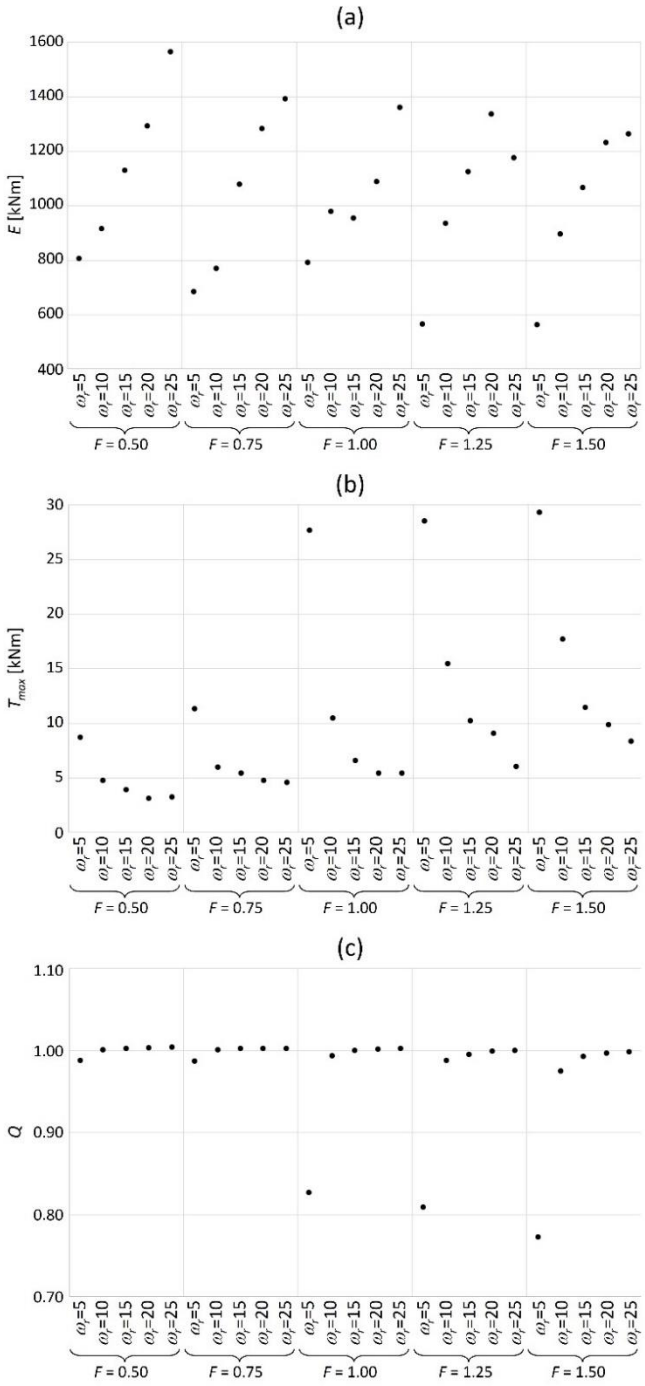


Fig. 4. Values of the selected responses (a) energy, (b) maximum torque, and (c) ring quality, as a function of $F$ [mm/s] and $\omega_r$ [rad/s].

The quality index $Q$ results to be positively influenced by an increase of the $\omega_r$ value, while it is negatively influenced by an increment of $F$. Moreover, for low $\omega_r$ values, the adverse effect of $F$ is more pronounced, meaning that the expected diameter growth is hindered. When increasing $F$, in fact, a higher radial penetration of the deformation is detectable, resulting in an increment of the material flow stress in the central part of the ring width. In this condition, the radial-axial material flow is

facilitated rather than the circumferential one, leading to a limited diametral growth. A reduction of $F$, instead, reduces the radial penetration enhancing the ring growth [18].

In consideration of the counter effect of $F$ and $\omega_r$ on the different responses, these latter were arranged in an objective function allowing to find an optimized combination of the process parameters, reducing at the same time energy, maximum torque, process time by maintaining a high quality.

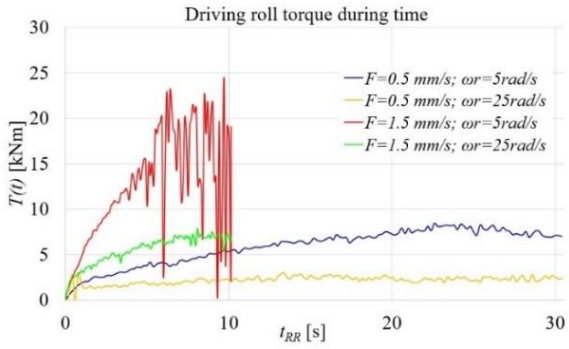


Fig. 5. $T(t)$ during process time for different combinations of $F$ and $\omega_r$.

## 4. Objective function definition and minimization results

With the aim of making the several responses comparable one to each other in the definition of the objective function, they were normalized by dividing each response value by its maximum as described in Eqs. (12), (13), and (14); the subscript $i$ represents the $i$-th simulation.

$$E_{norm\_i} = E_i / max(E_i) \quad (12)$$

$$T_{max\ \_norm\_i} = T_{max\ \_i} / max\left(T_{max_i}\right) \quad (13)$$

$$t_{RR\_norm\_i} = t_{RR\_i} / max\left(t_{RR_i}\right) \quad (14)$$

Table 3 reports the values of $t_{RR}$ and $t_{RR\_norm}$.

Table 3. Effective and normalized process time depending on $F$.

| $F$ [mm/s] | $t_{RR}$ [s] | $t_{RR\_norm}$ |
|---|---|---|
| 0.5 | 30.40 | 1.00 |
| 0.75 | 20.27 | 0.67 |
| 1.00 | 15.20 | 0.50 |
| 1.25 | 12.16 | 0.40 |
| 1.50 | 10.13 | 0.33 |

As previously reported, the closer the value of $Q$ to the unity, the better is the ring quality. Since from Eq. (11), $Q$ can assume values greater than one, it was normalized by calculating the absolute value of its difference with the unity (Eq. (15)).

$$Q_{norm} = |1 - Q| \quad (15)$$

A multi-variable regression allowed to define a second order function of the process parameters for each normalized response. Figure 6 shows the contour plots of the regression models of $E_{norm}$, $T_{max\_norm}$, $Q_{norm}$, and $t_{RR\_norm}$, as a function of $F$ and $\omega_r$. Similar trends to those of Figure 4 are observable.

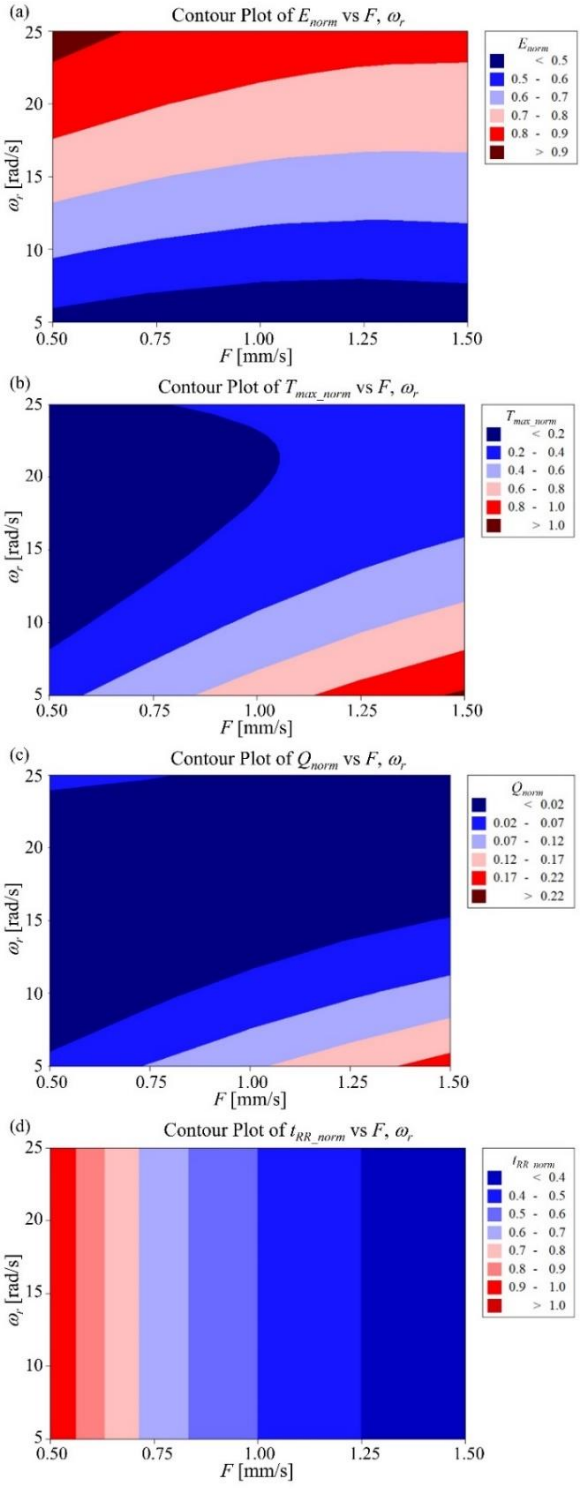


Fig. 6. Contour plots of (a) $E_{norm}$, (b) $T_{max\_norm}$, (c) $Q_{norm}$, and (d) $t_{RR\_norm}$ as a function of $F$ and $\omega_r$.

The objective function $f_{obj}$ was then defined as the sum of the normalized terms, as reported in Eq. (16), while its contour plot is represented in Figure 7.

$$f_{obj} = E_{norm} + T_{max\ \_norm} + Q_{norm} + t_{RR\_norm} \quad (16)$$

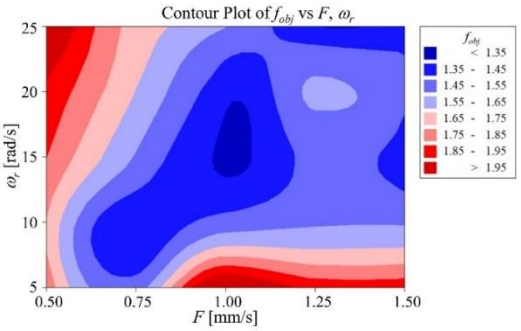


Fig. 7. Contour plot of the objective function to be minimized.

A first outcome of this study is that, even in presence of responses having their minimum on the domain boundaries, $f_{obj}$ shows an internal minimum (the blue area of Figure 7). Due to the counter effect of RR parameters on the outputs, $E$ and $t_{RR}$ on one side while $T_{max}$ and $Q$ on the other, the presence of the internal minimum permits a profitable inputs optimization. Since the purpose of this preliminary analysis was to confirm the suitability of the proposed methodology, equal weighted responses was considered. The $f_{obj}$ minimum value is lower than 1.35, corresponding to a feed rate $F_{\_opt}$ = 1.05 [mm/s] and a ring rotational speed $\omega_{r\_opt}$ = 17.0 [rad/s] (Figure 7). Referring to Figure 6, it is possible to find the correlated ranges' values of $E_{norm}$ (0.6 - 0.8), $T_{max\_norm}$ (0.2 - 0.4), and $Q_{norm}$ (lower than 0.02); corresponding to ranges of 940 – 1200 [kNm] for $E$, 5850 - 11700 [Nm] for $T_{max}$, and 379 - 395 [mm] for $D_{f\_sim}$. The optimized process time $t_{RR}$ is around 14.5 [s]. In order to test the results of the proposed optimization methodology, a FEM RR simulation using the optimized values ($F_{opt}$, $\omega_{r\_opt}$) was performed. The responses obtained were: $E$ = 1040 [kNm], $T_{max}$ = 7040 [Nm] and $D_{f\_sim}$ = 387 [mm]; revealing a maximum saving of 26 % and 40 % for the energy and the torque respectively, by maintaining the highest quality level ($Q_{norm}$ < 0.02). The simulated outputs considerably match the minimization outcomes, demonstrating the applicability of the proposed methodology.

## 5. Conclusions and future works

In this paper, a multi-objective optimization methodology for increasing the sustainability of energy-consumptive processes has been presented. Once individuated the process outputs mainly affecting the environmental aspects, their variation dependance respect to the process parameters has been analyzed. This allowed to arrange them in an objective function, that, once minimized, furnished the optimized values of the process parameters. The analyzed case refers to the ring rolling process. Energy request, maximum torque, ring quality, and process time has been individuated as the most interesting responses, leading to the identification of working parameters able to limit the energy consumption while maintaining a high level of product quality. In this preliminary study equal weights were assigned to the responses. To consider different importance of them, additional studies could be performed by employing a non-equal weighting strategy in Eq. (16). This would modify the objective function by shifting its minimum along the analyzed domain, altering the optimized RR parameters values. In this regard, a further sensitivity analysis of weights' effects on optimization results should be executed as well. Moreover, ring rolling simulations are time consuming and this limits the total number of feasible tests in an actual industrial application. Further analyses, implementing analytical models and artificial intelligence techniques, will therefore be carried out by correlating them to supplementary experimental validation. The preliminary application of the proposed methodology also proves to be useful also for studying different production processes.

## References

[1] Abeni A, Cappellini C, Attanasio A. A novel 2D micromilling FEM simulation strategy to otpimize the flow stress law of IN625. Proc. CIRP 2023;117:432-437.
[2] Satyajit M, Jagadish Chandra M, Ravi P. A review on life cycle assessment approach on thermal power generation. Mater. Today: Proc. 2022;56(2):791-798.
[3] Litos L, Patsavellas J, Afy-Shararah M, Salonitis K. An investigation between the links of sustainable manufacturing practices and innovation. Proc. CIRP 2023;116:390-395.
[4] Rauch E, Rofner M, Cappellini C, Matt D. Towards sustainable manufacturing: A case study for sustainable packaging redesign. In: Ivanov V, Trojanowska J, Pavlenko I, Rauch E, Peraković D, editors. Advances in Design, Simulation and Manufacturing V. DSMIE 2022. Lecture Notes in Mechanical Engineering. Springer, Cham. p. 84-93.
[5] Allwood JM, Tekkaya AE, Stanistreet TF. The development of ring rolling technology - Part 2: Investigation of process behaviour and production equipment. Steel Res. Int. 2005;76(7):491-507.
[6] Ryttberg K, Knutson Wedel M, Recina V, Dahlman P, Nyborg L. The effect of cold ring rolling on the evolution of microstructure and texture in 100Cr6 steel. Mater. Sci. Eng. A 2010;527(9):2431-2436.
[7] Yeom JT, Kim JH, Park NK, Choi SS, Lee CS. Ring-rolling design for a large-scale ring product of Ti-6Al-4V alloy. J. Mater. Process. Technol. 2007;187-188:747-751.
[8] Allwood JM, Tekkaya AE, Stanistreet TF. The development of ring rolling technology. Steel Res. Int. 2005;76(2-3):111-120.
[9] Eruç E, Shivpuri R. A summary of ring rolling technology-I. Recent trends in machines, processes and production lines. Int. J. Mach. Tools Manuf. 1992;32(3):379-398.
[10] Mamalis AG., Johnson W, Hawkyard JB. Pressure Distribution, Roll Force and Torque in Cold Ring Rolling. J. Mech. Eng. Sci. 1976;18(4):196-209.
[11] Lim T, Pillinger I, Hartley P. A finite-element simulation of profile ring rolling using a hybrid mesh model. J. Mater. Proces. Technol. 1998;80-81:199-205.
[12] Kim N, Machida S, Kobayashi S. Ring rolling process simulation by the three dimensional finite element method. Int. J. Mach. Tools Manuf. 1990;30(4):569-577.
[13] Pressas IS, Papaefthymiou S, Manolakos DE. Evaluation of the roll elastic deformation and thermal expansion effects on the dimensional precision of flat ring rolling products: A numerical investigation. Simul. Model. Pract. Theory 2022;117:102499.
[14] Wang ZW, Fan JP, Hu DP, Tang CY, Tsui CP. Complete modeling and parameter optimization for virtual ring rolling. Int. J. Mech. Sci. 2010;52(10):1325-1333.
[15] Qian D, Hua L. Blank design optimization for stepped-section profile ring rolling. Sci. China Technol. Sci. 2010;53(6):1612-1619.
[16] Zhu X, Liu D, Yang Y, Hu Y, Zheng Y. Optimization on cooperative feed strategy for radial-axial ring rolling process of Inco718 alloy by RSM and FEM. (2016) Chinese J. Aeronaut. 2016;29(3):831-842.
[17] Allegri G, Giorleo L. Ring rolling speed rolls optimization to improve ring quality and reduce production time. J. Mech. Eng. Sci. 2020;14(1):6272-6284.
[18] Zhuo G, Hua L, Lan J, Qian DS. FE analysis of coupled thermo-mechanical behaviors in radial–axial rolling of alloy steel large ring. Comp. Mater. Sci. 2010;50:65-76.